Catalysis Today 255 (2015) 87–96

Contents lists available at ScienceDirect

Catalysis Today

journal homepage: www.elsevier.com/locate/cattod

Solubility of greenhouse and acid gases on the [C_4mim][$MeSO_4$] ionic liquid for gas separation and CO_2 conversion

Fèlix Llovell[a,*], Mariana B. Oliveira[b], João A.P. Coutinho[b], Lourdes F. Vega[a,c]

[a] MATGAS Research Center, Campus de la UAB, 08193 Bellaterra, Barcelona, Spain
[b] CICECO, Chemistry Department, University of Aveiro, Campus de Santiago, 3810-193 Aveiro, Portugal
[c] Carburos Metálicos/Air Products Group, C/ Aragón 300, 08009 Barcelona, Spain

ARTICLE INFO

Article history:
Received 13 November 2014
Received in revised form
29 December 2014
Accepted 31 December 2014
Available online 10 March 2015

Keywords:
Ionic liquids
Gas separation
CO_2 conversion
Soft-SAFT
Selectivity

ABSTRACT

Ionic liquids (ILs) are an exciting class of compounds of high interest from a technological point of view. One of the applications that is raising more interest is their possible use as solvents to carry out the conversion of CO_2 into more valuable compounds. Theoretical approaches provide an attractive option to screen ILs properties and give quick answers to guide the experiments, becoming a crucial tool for process design. This work illustrates a practical example based on the solubility of greenhouse and acid gases on the butylmethylimidazolium methylsulfate [C_4mim][$MeSO_4$] IL, in order to study its feasibility for gas separation and conversion. A simple but reliable molecular model is presented for the ionic liquid based on structural information and molecular simulations, and coarse-grained models are used to model the different gases. The absorption of relevant gases for the separation/conversion process (CO_2, CH_4, CO, H_2, SO_2, H_2S) in [C_4mim][$MeSO_4$] is modeled and compared with experimental data using a minimum amount of binary data. From this information, the ternary diagrams of [C_4mim][$MeSO_4$] with CO_2 and the acid gases SO_2 and H_2S are predicted, and the selectivity of CO_2 by respect all the gases is evaluated, with particular attention to the contaminants above mentioned.

1. Introduction

In the last 15 years, ionic liquids (ILs) have drawn academic and commercial attention due to their unusual chemical and physical properties that make them valuable alternatives to traditional compounds and solvents for different applications [1]. ILs are practically non-volatile, present a wide liquid range and are not flammable, among other characteristics. A considerable volume of research and review work has been published addressing their valuable properties and their design for a specific application by choosing the appropriate cation/anion combination. This design is provided through a previous systematic thermophysical characterization, which is a key requirement for practical applications. Experimental measurements are required to do this task, but they can hardly explore all the ranges of temperature and pressure of application without an important economic and timing penalty.

One of the current potential applications of ILs is its use as a solvent for carbon dioxide (CO_2) capture and separation [2,3]. CO_2 usually comes as a residue from plant effluent streams, mixed with other greenhouse gases (CH_4, CO) or hazardous pollutants, such as H_2S and SO_2. This process can be seen as an alternative to the conventional technology of using chemical absorption through an aqueous solution of amines, which has important drawbacks, including loss of solvent, corrosion of facility, and high energy demand regeneration of the absorbent [4]. ILs are a possible kind of novel media that, with an appropriate selection, could result in a non-contaminated target gas, particularly attractive for the separation of these gases. The resulting purified CO_2 can be further transformed into useful compounds employing the same ILs as catalysts/reaction media [5], what is of paramount importance from a standpoint of green chemistry. Additionally, supercritical carbon dioxide in combination with ILs can be used in continuous green biocatalytic processes [6,7]. In this manner, CO_2 is converted from a residue into an added value compound or into a catalytic co-solvent. However, these processes require, as mentioned, a first gas separation step, which is a key element for an adequate posterior processing.

At the current moment, there is still a need for a further understanding of the dependence of the gas behavior on the IL microscopic structure in order to enhance its design. Molecular modeling techniques provide an excellent framework to progress on this field [8]. Among many equations of state (EoSs), the

* Corresponding author. Tel.: +34 935929950; fax: +34 935929951.
E-mail address: fllovell@matgas.org (F. Llovell).

http://dx.doi.org/10.1016/j.cattod.2014.12.049
0920-5861/

soft-SAFT EoS [9] provides a physically grounded theoretical approach to describe the thermophysical properties and phase behavior of ILs and their mixtures in good agreement with the experimental data [10–12]. Hence, the purpose of this work is to exploit the possibilities of soft-SAFT as a powerful tool for the description of the behavior of ILs and similar compounds, by exploring their ability to solubilize CO_2 and several other contaminant gases in them. In particular, we have focused our efforts in developing a theoretical semipredictive framework to study the potential application of the butylmethylimidazolium methylsulfate, [C_4mim][$MeSO_4$], IL for gas separation and conversion purposes.

Alkyl sulfate ILs have been recently subject of attention since they are halide-free ILs that can be used as an alternative to the widely investigated anion-fluorinated ILs, such as those with hexafluorophosphate, tetrafluoroborate or bis(trifluoromethylsulfonyl)imide as anions, considering their low cost, ease of preparation, wide electrochemical window, and air stability [13]. They can be used in the halide-free synthesis of other ILs by metathesis [13], as well as in organocatalysis for the synthesis of dihydropyrimidinones and -thiones [14].

In order to consider the use of this family of ILs for CO_2 separation and conversion processes, it is fundamental to know and understand the gas solubility behavior when these ILs are used as solvents. Previous works have focused on the experimental measurements of the solubility of various gases in [C_4mim][$MeSO_4$]. Some of these studies also present interesting results obtained from theoretical modeling approaches. For instance, Kumełan and co-workers presented solubility data for several gases in [C_4mim][$MeSO_4$] in wide temperature ranges for CO_2 [15], CH_4 [16], H_2 [17] and CO [17]. They used the extended Henry's law through the virial expansion proposed by Pitzer for the activity coefficients calculations to correlate the data. Of particular interest for the present contribution is the work done by Shiflett and co-workers [18–20], where the solubility of H_2S and SO_2 in [C_4mim][$MeSO_4$] was measured. They showed how the chemical absorption controlled the SO_2 solubility in the IL [18,20], and even presented phase equilibria data for the ternary systems composed of those gases, the IL and CO_2. A cubic equation of state, based on the SRK EoS but with up to 4 binary interaction parameters, was developed for the description of the high pressure phase equilibria of gases + ILs systems and was applied to describe the reported experimental data. These contributions have shown that [C_4mim][$MeSO_4$] enhances significantly the selectivity of the CO_2/SO_2 and CO_2/H_2S mixtures, being a potential candidate to substitute classical solvents.

This article is organized as follows: a short description of the main features of the soft-SAFT equation is exposed in the next section. Then, the different molecular models used to describe the gases and the selected IL of this work are explained appropriately, highlighting the assumptions made for each particular case. The results section includes a variety of phase diagrams showing the solubility of the different gases in [C_4mim][$MeSO_4$], the calculation of the Henry's constant for each case and the selectivity to separate the other gases from CO_2. Additionally, particular attention is given to the removal of acid gases by studying the ternary diagram of these mixtures with CO_2 and the IL, looking for the best separation conditions. Finally, some concluding remarks are given in the last section.

2. Methodology

The soft-SAFT equation [9] is a well-established variant of the original Statistical Associating Fluid Theory (SAFT) equation of state [21]. Based on Wertheim's first-order perturbation theory [22–24], it provides a framework in which the effects of molecular shape and intermolecular interactions on the thermodynamic properties of a system are explicitly considered. The equation calculates the total free energy of the system as a sum of different independent contributions that account for several molecular effects. For associating and polar molecules, the soft-SAFT approach calculates the Helmholtz energy of the system as a sum of an ideal contribution, A^{ideal}, a reference term, A^{ref}, for the attractive and repulsive forces between the segments that form the molecules, a chain contribution, A^{chain}, for the connectivity of the segments in the molecules, a contribution due to site-site intermolecular association, A^{assoc}, and a polar term, A^{polar}:

$$A^{total} - A^{ideal} = A^{res} = A^{ref} + A^{chain} + A^{assoc} + A^{polar}. \quad (1)$$

A^{res} is the residual Helmholtz energy density of the system. The reference term of the soft-SAFT EoS is given by a Lennard–Jones (LJ) spherical fluid, considering repulsive and attractive interactions of the monomers in a single contribution. This intermolecular potential includes the sphere (segment) diameter of the monomers σ_{ii} and the dispersive energy between segments ε_{ii}/k_B. The equation of Johnson et al. [25], adjusted to molecular simulations of Lennard–Jones monomers, is used here to calculate the free energy of this term.

In order to extend the LJ contribution to mixtures, it is necessary to apply the van der Waals one-fluid theory, due to the fact that the original reference term does not explicitly consider mixtures.

$$\sigma_m^3 = \frac{\sum_{i=1}^{n}\sum_{j=1}^{n} m_i m_j x_i x_j \sigma_{ij}^3}{\sum_{i=1}^{n}\sum_{j=1}^{n} m_i m_j x_i x_j}, \quad (2)$$

$$\varepsilon\sigma_m^3 = \frac{\sum_{i=1}^{n}\sum_{j=1}^{n} m_i m_j x_i x_j \sigma_{ij}^3}{\sum_{i=1}^{n}\sum_{j=1}^{n} m_i m_j x_i x_j}. \quad (3)$$

The unlike size σ_{ij} and energy ε_{ij}/k_B soft-SAFT molecular parameters are obtained with the modified Lorentz–Berthelot (LB) combining rules:

$$\sigma_{ij} = \eta_{ij}\left(\frac{\sigma_{ii}+\sigma_{jj}}{2}\right), \quad (4)$$

$$\varepsilon_{ij} = \xi_{ij}(\varepsilon_{ii}\varepsilon_{jj})^{1/2} \quad (5)$$

where ξ_{ij} and η_{ij} are the size and energy binary adjustable parameters, respectively. It is important to clarify that when both values are set to one, Eqs. (4) and (5) reduce to the classical LB combining rules and the model becomes predictive. Note that ξ_{ij} is equivalent to $(1-k_{ij})$, and η_{ij} is equivalent to $(1-l_{ij})$, the energy and size binary parameters most commonly used in classical equations of state.

The chain and association terms come from Wertheim's theory [22–24] and are formally identical in all SAFT equations:

$$A^{chain} = Nk_BT\sum_i x_i(1-m_i)\ln g_{LJ}, \quad (6)$$

$$A^{assoc} = Nk_BT\sum_i x_i\sum_a\left(\ln X_i^a - \frac{X_i^a}{2}\right) + \frac{M_i}{2}, \quad (7)$$

where N is the number of molecules, k_B is the Boltzmann constant and T is the temperature. The chain term is obtained using an equation fitted to molecular simulations of LJ chains [26]. The chain term includes the chain length parameter m_i, while the association term involves two additional parameters related to the volume (K^{HB}) and energy (ε^{HB}/k_B) of the association sites.

Eqs. (6) and (7) are expressed in a general form valid for n compounds. The only requirement to extend the treatment to mixtures is the evaluation of the cross-association volume ($K^{HB}{}_{ij}$) and energy ($\varepsilon^{HB}{}_{ij}/k_B$) parameters to account for the energy and volume of association between different compounds. In this work, the mean arithmetic of the cube root of $K^{HB}{}_{ij}$ and the geometric average for

$\varepsilon^{HB}{}_{ij}/k_B$ (in an analogous way as it is done for σ_{ij} and ε_{ij}/k_B) are used to obtain these values:

$$K_{ij}^{HB} = \left(\frac{\sqrt[3]{K_{ii}^{HB}} + \sqrt[3]{K_{jj}^{HB}}}{2} \right)^3, \quad (8)$$

$$\varepsilon_{ij}^{HB} = (\varepsilon_{ii}^{HB}\varepsilon_{jj}^{HB})^{1/2}. \quad (9)$$

The last term of the equation, A^{polar}, is a multipolar contribution included when fluids exhibit a polarity strength affecting the physical interactions in a significant way, as it is the case of the quadrupole in carbon dioxide. The calculation of this term is carried out following the methodology proposed by Gubbins and Twu [27] for spherical molecules and extended to chain fluids by Jog et al. [28]. The polarity effect is considered through a perturbative approach of the Helmholtz free energy density, written with the Padé approximation [29]. The reader is referred to previous bibliography for the implementation details [27–29]. The theory includes an effective quadrupole moment, Q, and the fraction of segments in the chain that contains this effective quadrupole, x_p. Both parameters are related by the following equation:

$$Q = Q_{\text{exp}} \cdot xp \quad (10)$$

where Q_{exp} is the experimental quadrupole moment of the molecule (C m^2).

3. Molecular models

The success of a molecular-based equation of state relies on the development of a simple but accurate molecular model, able to capture the main physical features of the compound through a coarse-grained approach, while still being manageable in terms of computing time. Hence, it is necessary to develop a model for each one of the compounds involved in this work (gases and IL), within the soft-SAFT framework, that meets these requirements.

Methane (CH_4) and hydrogen (H_2) are non-associating molecules. Hydrogen is very stable and non-reacting, while methane does not exhibit any type of anisotropic short range attractive interactions. As a consequence, both molecules are modeled as non-associating compounds (in other words the terms A^{assoc} and A^{polar} in Eq. (1) are set to zero). Moreover, methane is set to be a spherical molecule, represented by a LJ sphere ($m = 1$), which means that the chain term is also zero. Carbon monoxide (CO) is almost an entirely non-polar molecule, as it can be seen by its very low dipole moment ($\mu = 0.12$ D). Hence, it is possible to also model this molecule as a non-associating system with only three parameters m, σ, and ε/k_B. This assumption is based on a previous work [30], where it was shown that a non-associating model for CO was accurate enough to provide very good results to describe the solubility of this gas in [PF_6]-based ILs. The very slight polar character of the molecules is implicitly considered through the values of these parameters. The final sets of molecular parameters of these three molecules were taken from previous contributions [30–32] and are included in Table 1 for completeness.

Carbon dioxide (CO_2) is modeled as a LJ chain in which explicit quadrupolar interactions are taken into account. Consequently, in addition to the molecular parameters described above, the experimental quadrupole moment, Q, and the fraction of segments in the chain that contains the quadrupole, x_p, are required. x_p was fixed to 1/3 for CO_2 to mimic molecules as three segments with a quadrupole in one of them, respectively. The final set of molecular parameters is taken from Ref. [33].

Hydrogen sulphide (H_2S) is modeled as an associating molecule with 3 interaction sites: 2 sites of type H for the hydrogen atoms and 1 site of type e for the electronegativity of the sulphur, with only e–H interactions allowed. Sulfur dioxide (SO_2) is represented by a LJ chain with two associating sites of different nature (positive–negative) to mimic in an effective manner the nature of the dipole moment of the molecule. Both molecules were described in detail in Ref. [34].

The modeling of ILs with soft-SAFT is based on the assumption that dispersion forces, specific steric interactions and, possibly, the formation of short-lived ion pairs reduce the ionic character of ILs, as observed in molecular simulations [35]. Based on this principle, they are modeled as a single chain, where the cation and the anion are together and with an anisotropic interaction between different pairs. This anisotropic and strong interaction is taken into account in a SAFT approach through association sites, which need to be specified. Hence, [C_4mim][$MeSO_4$] is presented within the soft-SAFT framework as a homonuclear chain-like molecule with two associating sites in each molecule that describe the specific cation–anion interactions due to the charges and the asymmetry: one site A, representing the interaction of the anion oxygen with the cation, and one site B, representing the anion delocalized charge, due to the second anion oxygen atom. Only AB interactions between different IL molecules are permitted.

The molecular parameters for all the gases were fitted to their phase equilibrium liquid density and vapor pressure. Conversely, due to their negligible vapor pressure, the molecular parameters of [C_4mim][$MeSO_4$] were fitted to temperature–density data at atmospheric pressure. In the present contribution, only the final set of parameters for each compound is included in Table 1, along with the reference of the original contributions where this optimization was made [30,31,33,36]. It is important to remark that it is possible to find several sets of parameters that accurately describe the temperature–density equilibrium of the IL. However, we have chosen the most meaningful set of parameters from a physical and transferable point of view, and have tested their validity reproducing not only the liquid density of the IL, but also the solubility behavior in the presence of water and short alcohols [36].

4. Results: solubility of gases on [C_4mim][$MeSO_4$]

In this section, a descriptive summary of the results achieved in this thermodynamic study of the behavior of gases on [C_4mim][$MeSO_4$] is given, including details about the different features observed.

Table 1
Soft-SAFT EoS molecular parameters for the compounds studied in this work.

	m_i	σ_{ii} (Å)	ε_{ii}/k_B (K)	$\varepsilon_{ii}^{HB}/k_B$ (K)	K_{ii}^{HB} (Å^3)	10^{40} Q (C m^2)	Number assoc. sites	Ref.
CO_2	1.571	3.184	160.20			4.40	–	Dias et al. [33]
CO	1.466	3.170	85.60			–	–	Llovell et al. [30]
CH_4	1.000	3.728	147.2			–	–	Pàmies and Vega [31]
H_2	0.4874	4.244	33.85			–	–	Florusse et al. [31]
H_2S	1.706	3.060	225.80	673.8	500.6	–	3	Llovell et al. [34]
SO_2	2.444	2.861	228.3	1130	601.0	–	2	Llovell et al. [34]
[C_4mim][$MeSO_4$]	6.010	3.786	400.0	4000	2250	–	2	Mac Dowell et al. [36]

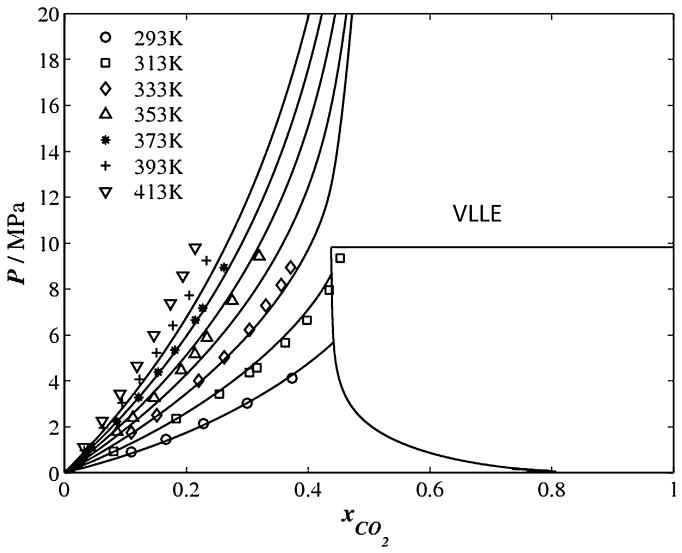

Fig. 1. Solubility of CO_2 in [C_4mim][$MeSO_4$] at T = 293.20 K (circles), T = 313.25 K (squares), T = 333.10 K (diamonds), T = 353.10 K (triangles), T = 373.10 K (stars), T = 393.10 K (crosses) and T = 413.10 K (inverted triangles), with no binary interaction parameters. Symbols are experimental data [15], while the curves, including the VLLE gap, are the soft-SAFT predictions.

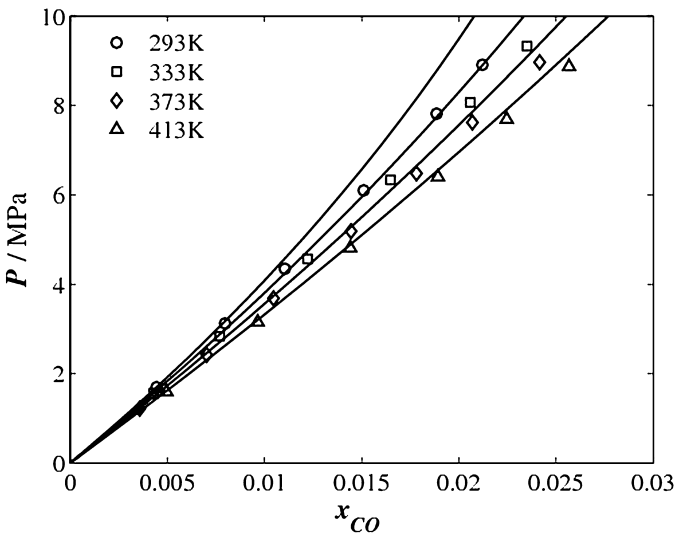

Fig. 2. Solubility of CO in [C_4mim][$MeSO_4$] at T = 293.15 K (circles), at T = 333.15 K (squares), at T = 373.15 K (diamonds), at T = 413.20 K (triangles), with a binary temperature dependent η parameter (see Table S1). Symbols are experimental data [17], while the curves are the soft-SAFT EoS calculations.

4.1. Carbon dioxide solubility

The first system addressed with soft-SAFT is the CO_2 + [C_4mim][$MeSO_4$]. Experimental data were available for the CO_2 solubility at seven different temperatures, covering a wide range from 293 K to 413 K [15].

As done in previous studies, where the soft-SAFT was applied to describe the CO_2 solubility in other ILs [10,37–39], the LB combining rules were firstly used to predict the phase diagram of the mixture and, in case of disagreement with the experimental data, the energy binary parameter ξ was fitted to one data isotherm and used, when possible, to predict the rest of the isotherms. In this case, the predicted phase diagram (no binary parameters used) shown in Fig. 1 is in very good agreement with the available data at temperatures up to 353 K, while some deviations appear at higher values. Considering the fact that the working industrial conditions for gas separation are in the low range of temperatures (298–333 K), where better agreement is achieved, we have decided to preserve this model, highlighting the predictability of the approach. More interestingly, the model also predicts a vapor–liquid–liquid equilibrium (VLLE) region at high IL concentrations, confirming the findings of Shiflett and Yokozeki [18]. In our predictions, the VLLE is even wider than the one predicted by those authors, reaching an upper critical end point (UCEP) at 319.6 K. This high degree of immiscibility will have an important impact when studying ternary mixtures with a second gas for separation purposes.

4.2. Carbon monoxide solubility

The system composed by carbon monoxide and [C_4mim][$MeSO_4$] is an example of a mixture characterized by weak energy interactions and strong size differences between both components. Consequently, the experimental solubility data of the gas in the IL is dominated by entropic effects and shows very low values that increase with temperature, contrarily to the CO_2 case [17]. As a consequence, the use of a size binary parameter η, instead of the energy parameter ξ, is recommended to account for the asymmetry of this mixture. In Fig. 2, the system CO + [C_4mim][$MeSO_4$] is modeled with soft-SAFT using a temperature-dependent size binary parameter (and keeping the energy parameter to unity), obtaining a very good description of the phase equilibria for temperatures between 293.15 and 413.2 K. The size binary parameters are all close to unity and, for the three higher temperatures, they follow a linear temperature dependency. Their values are reported in Table S1, in the Additional Supporting Information document.

Supplementary material related to this article can be found, in the online version, at http://dx.doi.org/10.1016/j.cattod.2014.12.049.

4.3. Hydrogen solubility

The H_2 solubility in [C_4mim][$MeSO_4$] has also been described with soft-SAFT at the conditions at which experimental data were available (293.3, 333.15, 373.1, and 413.2 K) [17]. Soft-SAFT had already been used to model the H_2 solubility in [C_6mim][Tf_2N] [11] without any binary parameter needed, and in [C_4mim][PF_6] [40] with a temperature independent size binary parameter. Preliminary calculations showed a similar behavior to that observed for CO. The energy binary parameter seems not to have a major impact in the solubility modeling results – an expected outcome, as the interactions between H_2 and the IL are minor, as deduced from the experimental low solubility data of this gas in the IL. A size binary parameter is again necessary to account for the difference in size between the two components. The experimental data at 333.15 K were used in the binary parameter regression. A value of η = 0.978 obtained was found to provide good predictive results when transferred to the remaining three temperatures for which experimental data were available, so it was keep constant and independent of the temperature. The soft-SAFT results for the H_2 solubility in [C_4mim][$MeSO_4$] are shown in Fig. 3.

4.4. Methane solubility

Once again, methane is a gas exhibiting low solubility on [C_4mim][$MeSO_4$], as it can be seen from the experimental data from Kumełan et al. [16]. The available data, in a range of temperatures between 293.15 and 413.2 K, also reveal little temperature effect. These results had been previously seen for other CH_4 + IL systems, namely for [C_2mim][CH_3OHPO_2], for which experimental measurements of the CH_4 solubility were presented in the work

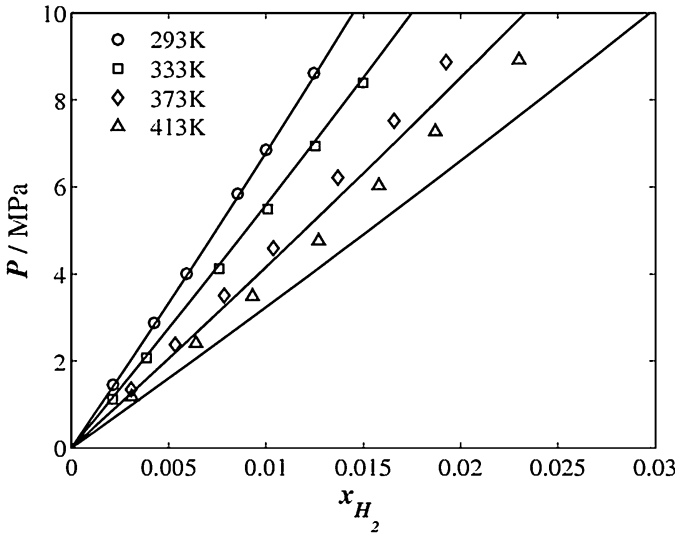

Fig. 3. Solubility of H_2 in [C_4mim][$MeSO_4$] at T = 293.30 K (circles), T = 333.15 K (squares), T = 373.10 K (diamonds) and T = 413.20 K (triangles) with a binary parameter η = 0.978. Symbols are experimental data [16], while the curves are the soft-SAFT EoS calculations.

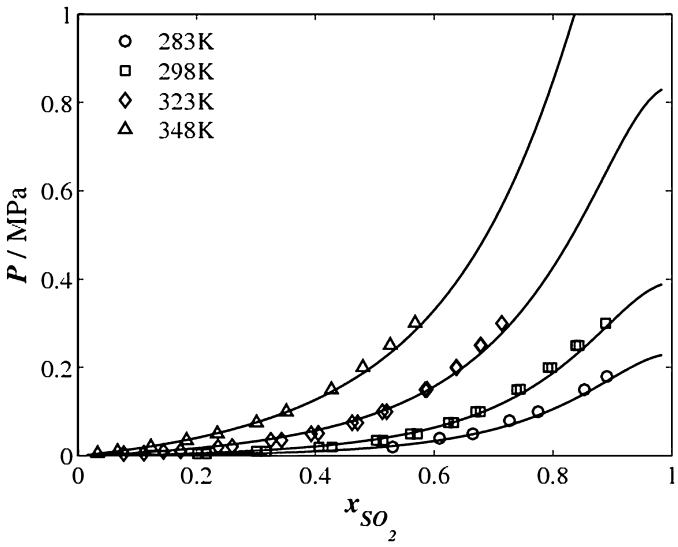

Fig. 5. Solubility of SO_2 in [C_4mim][$MeSO_4$] at T = 283.15 K (circles), T = 298.15 K (squares), T = 323.15 K (diamonds) and T = 348.15 K (triangles) with an energy binary parameter ξ = 1.048. Symbols are experimental data [20], while the curves are the soft-SAFT EoS calculations.

of Pereira et al. [38]. In that work, the soft-SAFT was applied to describe the experimental data using a temperature dependent size binary parameter. For the CH_4 + [C_4mim][$MeSO_4$] system considered in this work, the same hypothesis were taken: the energy interactions between the two components are too small and hence the incorporation of an energy binary interaction parameter is not needed; on the contrary, the strong size differences between the segments constituting CH_4 and [C_4mim][$MeSO_4$] have to be considered using a temperature dependent size binary interaction parameter, obtained by fitting to the available experimental data (as was done in Section 4.2 for CO). The binary interaction parameter values, listed in Table S1, are very similar and slightly higher than unity. In Fig. 4, the description of the methane solubility in [C_4mim][$MeSO_4$] is provided, showing very good agreement between the soft-SAFT modeling results and the experimental data [16].

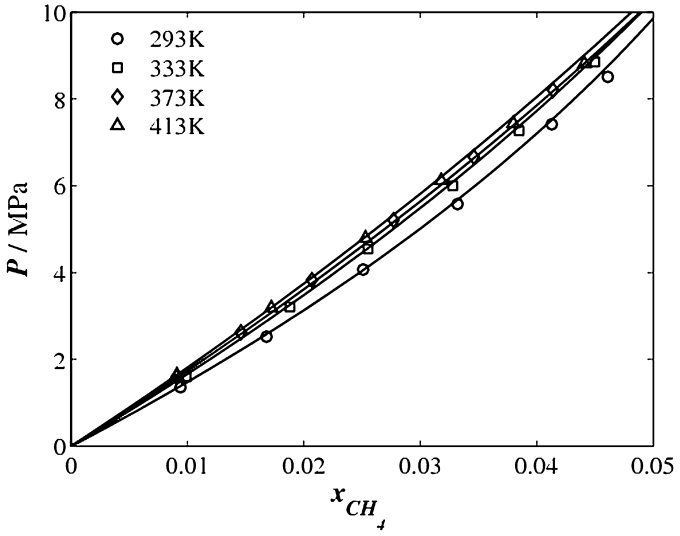

Fig. 4. Solubility of CH_4 in [C_4mim][$MeSO_4$] at T = 293.15 K (circles), T = 333.15 K (squares), T = 373.15 K (diamonds) and T = 413.20 K (triangles) with a binary temperature dependent η parameter (see Table S1). Symbols are experimental data [17] and the curves are the soft-SAFT EoS calculations.

4.5. Acid gases (H_2S and SO_2) solubility

In this sub-section, the solubility of the acid gases H_2S and SO_2 in [C_4mim][$MeSO_4$] is described. Here, it is important to note that both gases exhibit short range physical interactions, which are described through the addition of association sites. In addition, both molecular simulations and quantum studies have shown that cross-association interactions with the IL are present in the mixture [41]. This feature must be represented by the molecular model in order to have a reliable picture of the physical behavior of the mixture. This effect will be accounted for by considering cross-association between the acid gases and the IL. Cross-association values have been obtained using Eqs. (8) and (9) without any further adjustment, in order to keep the model as predictive as possible.

The soft-SAFT molecular model of [C_4mim][$MeSO_4$] contains two sites (one A site and one B site). For SO_2, two sites of different nature mimic the effect of the dipole moment. For the mixture with the IL, we have taken into account interactions between the negative site of SO_2 (site −) and the A site of the IL (pair A, −), and between the positive site of SO_2 (site +) and the B site of the IL (pair B, +). For the H_2S case, the molecule was modeled using three associating sites: one site e′ representing the sulfur negative charge and two H′ sites representing the two hydrogen atoms of the molecule. Hence, we consider cross-association interactions between the sulfur atom of H_2S (site e′) and the A site of the IL (pair A, eí) and between the two hydrogen atoms of H_2S (sites H′) and the B site of the IL (pair B, H′). Other cross-associating possibilities (pairs B, e′ and A, H′) are not allowed. The possible cross interactions have been established based on previous results obtained for the other anions, such as $[Tf_2N]^-$, $[PF_6]^-$ and $[BF_4]^-$ with these acid gases, where excellent predictions for VLE and LLE diagrams were obtained following the same cross-associating interactions hypothesis [34].

Results concerning modeling the solubility of the acid gases SO_2 and H_2S in [C_4mim][$MeSO_4$] are presented in Figs. 5 and 6, respectively. The SO_2 + [C_4mim][$MeSO_4$] is depicted in Fig. 5, in a range of temperatures going from 283 K till 348 K. As it can be observed, the agreement reached between the soft-SAFT calculations and the experimental data [20] is excellent at all conditions. These results have been obtained using a binary energy parameter ξ = 1.048. The ξ value has been fitted to an intermediate

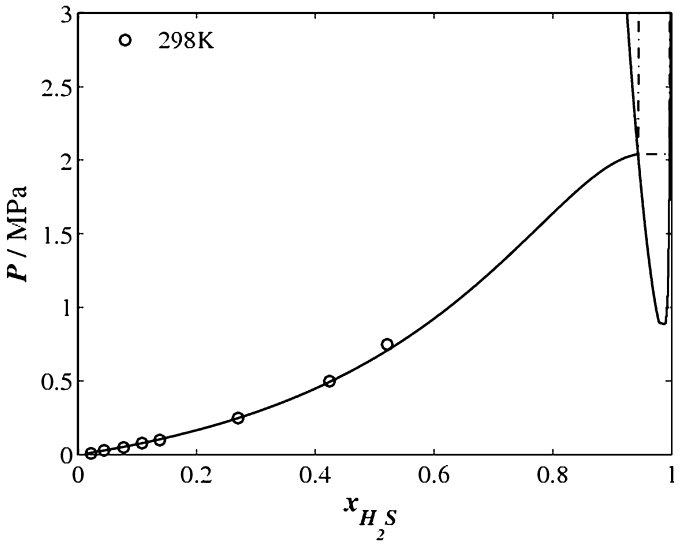

Fig. 6. Solubility of H_2S in [C_4mim][$MeSO_4$] at T = 298.15 K (circles) with an energy binary parameter ξ = 0.980. The curves represent the soft-SAFT VLE calculation and VLLE gap prediction of the mixture. The symbols represent experimental data [19].

temperature of 323.15 K and transferred to other temperatures. In Fig. 6, the H_2S + [C_4mim][$MeSO_4$] is plotted. Shiflett and co-workers [19] had measured this system at 298 K and they had found a very narrow liquid–liquid immiscibility gap at compositions very close to pure H_2S. Using soft-SAFT, the solubility of H_2S has been quantitatively described using an energy binary parameter ξ = 0.980, which is very close to unity. Additionally, the VLLE region has been predicted in reasonable agreement with the findings of Shiflett et al. [19], although our predictions indicate a wider range of immiscibility (starting at a H_2S composition of 0.944, approximately, at 298.15 K). The VLLE line has been included, finding a lower critical end point (LCEP) at 268.1 K and an upper critical end point (UCEP) at 375.6 K. This behavior is in contrast to the one exhibited by the CO_2 + [C_4mim][$MeSO_4$] mixture, which had a very wide immiscibility gap but ending at a relatively low temperature (319.6 K). Here, the immiscibility gap remains narrow and only occurring at very high compositions of H_2S, but it reaches a considerable higher temperature.

4.6. Selectivity

In order to address the appropriateness of a solvent for application in gas separation processes, it is necessary to evaluate its gases selectivity. The selectivity can be easily calculated through Henry's constants representing volatility, which relate the amount of gas dissolved in the solvent at a constant temperature to the fugacity of that gas in equilibrium with the solvent.

$$h_{i,L}(T,p) = \lim_{x_{i\to 0}} \frac{f_i^L}{x_i} \tag{11}$$

The soft-SAFT equation of state is used to compute data for the limiting slope as the solubility approaches zero. Henry's law constants for the studied gases in the selected ionic liquid, at two different temperatures, 293.15 K and 333.15 K, are reported in Table 2. Here, it is important to mention that, in order to establish a comparison with the values reported in the literature, we have converted the Henry's constant results from the molarity scale (as defined in Eq. (11)), to the molality (m) scale ($H_{i,L}(T,p) = \lim_{x_{i\to 0}}(f_i^L)/(m_{gas}/m^o)$, where m^o = 1 mol/kg, as it is defined in other bibliographic sources [15–17]). The values predicted are, in all cases, in excellent agreement with those reported in the literature [42], which are also included in Table 2. Henry's law constants for CO_2, H_2S and SO_2 are dramatically lower than those of the other gases, whose high values are in agreement with the very low solubility observed for H_2, CH_4 and CO in [C_4mim][$MeSO_4$].

Once the Henry's constants of all gases have been estimated, gases selectivity can be easily calculated as the ratio between the Henry's constants for each gas:

$$S_{CO_2/gas} = \frac{H_{gas}}{H_{CO_2}} \tag{12}$$

Results for all gases are displayed in Table 3. [C_4mim][$MeSO_4$] has a high selectivity for CO_2 separation from H_2, CH_4 and CO, a fact which was already quite evident seeing the low solubility of these three gases in the IL. Hence, [C_4mim][$MeSO_4$] can be recommended in separations processes with the objective of extracting CO_2 from streams containing these gases, in order to achieve a solution with a high concentration in CO_2, adequate to carry out the CO_2 conversion.

On the contrary, [C_4mim][$MeSO_4$] is not suitable to be used in the capture of CO_2 in process streams with high content of SO_2 and H_2S as contaminants, since, as depicted in Table 3, CO_2/SO_2 and CO_2/H_2S selectivity values are considerably low. These results are in agreement with the SO_2 and H_2S high solubility in [C_4mim][$MeSO_4$], also confirmed by the low Henry's constants of these two gases. However, the low values indicate that this solvent can effectively be used to recover those acid gases from gaseous effluents leaving the CO_2 in the gas phase free of contaminants. In other words, the feasibility of the gas separation by extractive distillation or selective absorption is high, as the gaseous absorption selectivity is the inverse value of that shown in Table 3.

$$S_{gas/CO_2} = \frac{H_{CO_2}}{H_{gas}} \tag{13}$$

Using Eq. (13), the selectivity of the SO_2/CO_2 separation is very high, while the H_2S/CO_2 separation is only moderate.

4.7. Ternary diagrams

Once the solubility of all the previous gases in [C_4mim][$MeSO_4$] has been modeled, the calculation of the selectivity values, as obtained from Eqs. (11)–(13) has allowed identification of the ability of the tested solvent for gas separation applications (from both the volatility and solubility perspective, depending on the gas mixture). As shown in the previous section, high CO_2 selectivity values

Table 3
Estimated CO_2 selectivities at 293.15 K and 333.15 K.

T/K	$S_{CO_2/CO}$	S_{CO_2/CH_4}	S_{CO_2/H_2}	S_{CO_2/H_2S}	S_{CO_2/SO_2}
293.15	56.55	21.24	96.30	0.082	0.00225
333.15	25.92	11.26	38.41	0.245	0.01353

Table 2
Estimated Henry's constants (MPa) for CO_2, CO, CH_4, H_2, H_2S and SO_2, at 293.15 K and 333.15 K (for each gas, first column shows results from this work, second column represents results from literature [42]).

T, K	H_{CO_2}		H_{CO}		H_{CH_4}		H_{H_2}		H_{H_2S}	H_{SO_2}
293.15	1.65	1.87	96.76	93.5	35.90	34.5	165.21	168.4	0.137	3.78×10^{-3}
333.15	3.47	3.51	92.07	88.8	39.68	38.8	136.79	131.8	0.411	2.23×10^{-2}

are achieved in most cases, showing that this IL can become a potential candidate for this purpose. However, more precise information can only be obtained if the phase behavior of the ternary mixture between the gas, CO_2 and the IL is known. In particular, it is important to (1) check the phase behavior of both gases together at the same conditions of temperature and pressure (2) check the selectivity variation as a function of the gas/CO_2 feed ratio, and (3) ensure that no undesirable effects occur at separation conditions (for instance, the expansion of the immiscibility gap of CO_2 found in the binary mixture).

We have focused our efforts in the separation of the two acid gases SO_2 and H_2S from CO_2, because of its interest for further conversion or other industrial applications and the current difficulty in carrying out this separation. The predictive capability of the soft-SAFT equation is used here to predict the phase behavior of the ternary mixture without using ternary mixture data.

The procedure to calculate the ternary mixture requires the previous evaluation of all the binary pairs. This includes the study of the phase behavior of the CO_2/SO_2 and the CO_2/H_2S mixtures. In Fig. 7a, the vapor–liquid equilibrium of CO_2/SO_2 at 3 different temperatures (263.15 K, 273.15 K and 333.15 K) has been plotted. Very good agreement with the available experimental data (taken from Refs. [43,44]), is obtained at all temperatures using a constant binary parameter $\xi = 1.065$, fitted to 273.15 K and used for the other two isotherms in a predictive manner. In Fig. 7b, the vapor–liquid equilibrium of CO_2/H_2S at 3 different pressures (2.96 MPa, 4.94 MPa and 6.91 MPa) is depicted. Here again, excellent agreement with the available experimental data [45] is obtained for all isobars using a constant binary parameter $\xi = 1.017$, fitted to the intermediate isobar and used for the other two in a predictive manner. It is interesting to note that the binary parameter value is close to unity, meaning that only a slight correction from the classical combining LB rules is needed.

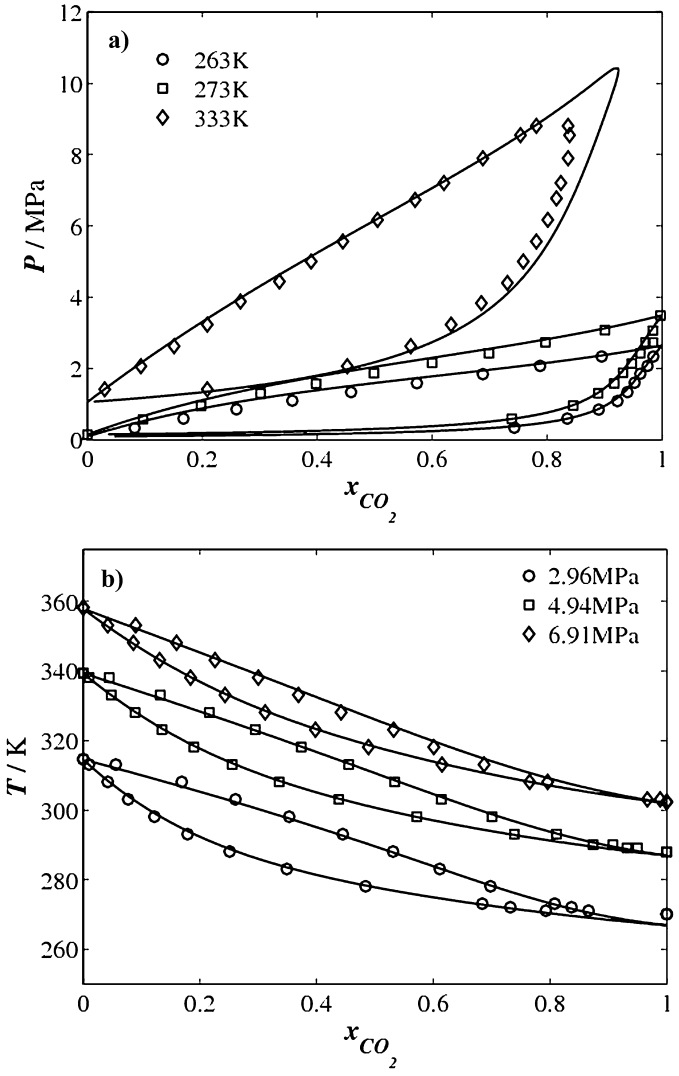

Fig. 7. Vapor–liquid equilibrium of CO_2/acid gases mixtures. (a) Pressure-composition CO_2/SO_2 diagram at $T = 263.15$ K (circles), $T = 273.15$ K (squares), $T = 333.15$ K (diamonds) with an energy binary parameter $\xi = 1.065$. (b) Temperature-composition CO_2/H_2S at $P = 2.96$ MPa (circles), $P = 4.94$ MPa (squares), $P = 6.91$ MPa (diamonds) with an energy binary parameter $\xi = 1.017$. Symbols are experimental data [43–45] while the curves are the soft-SAFT calculations.

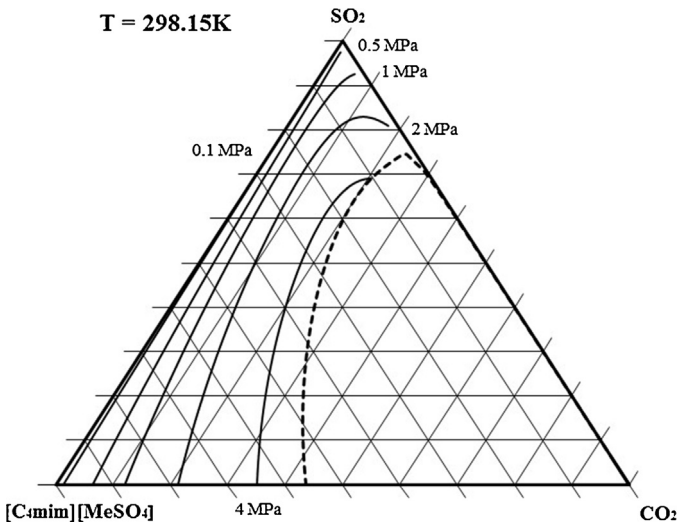

Fig. 8. Isothermal ternary phase diagram at $T = 298.15$ K predicted with soft-SAFT for the $CO_2/SO_2/[C_4mim][MeSO_4]$ mixture. The different full curves represent the calculation of different isobars at 0.1 MPa, 0.5 MPa, 1 MPa 2 MPa and 4 MPa, while the dashed curve represents the VLLE immiscibility area.

In Figs. 8 and 9, the ternary diagrams for the mixtures $CO_2 + SO_2 + [C_4mim][MeSO_4]$ (Fig. 8) and $CO_2 + H_2S + [C_4mim][MeSO_4]$ at 298.15 K (Fig. 9) are shown. In both cases, several isobars (full curves) are included in order to check the behavior of the mixture as a function of the pressure. The dashed

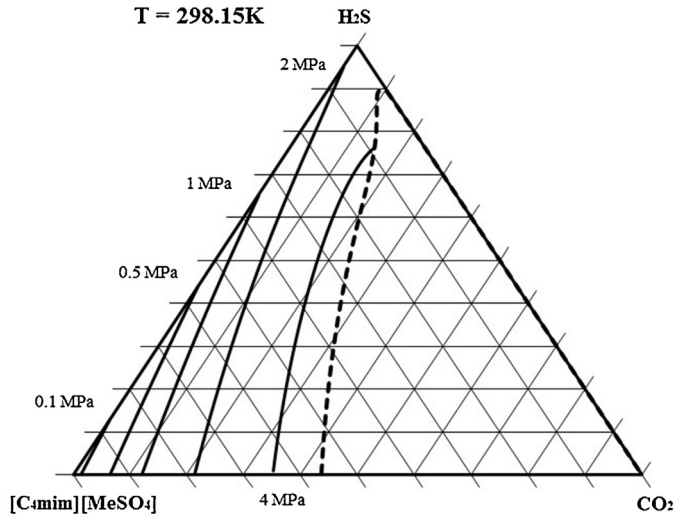

Fig. 9. Isothermal ternary phase diagram at $T = 298.15$ K predicted with soft-SAFT for the $CO_2/H_2S/[C_4mim][MeSO_4]$ mixture. The different full curves represent the calculation of different isobars at 0.1 MPa, 0.5 MPa, 1 MPa 2 MPa and 4 MPa, while the dashed curve represents the VLLE immiscibility area.

curve indicates the predicted vapor–liquid–liquid equilibrium (VLLE) three-phase line. As it can be seen, there is a big immiscibility region that comes from the immiscibility exhibited by the $[C_4mim][MeSO_4]+CO_2$ binary mixture. The results are similar for both mixtures, indicating that liquid–liquid immiscibility is achieved at high pressures when the concentration of IL reaches 50% or more depending, of course, of the CO_2/gas ratio. The results obtained for the SO_2 case compare well with the diagram predicted by Shiflett and Yokozeki with an SRK-type EoS [18], although we predict here a higher degree of immiscibility that could even be reached for SO_2 concentrations higher than 70%. No comparison can be made for the H_2S case, as the ternary diagram has not been shown in any contribution.

From the ternary diagram, it is possible to better evaluate the selectivity of the CO_2/SO_2 separation as a function of the addition of ionic liquid in the feed flow. In the previous section, it was shown that SO_2 is a more soluble gas and will become the solute of the mixture, while CO_2 is expected to remain alone in the gas phase. In order to compute the selectivity from the ternary mixture data, we will directly calculate the selectivity from the molar composition of the two gases in the liquid and vapor phases, in an expression analogous to Eq. (13):

$$S_{gas/CO_2} = \frac{(y_{CO_2}/x_{CO_2})}{(y_{gas}/x_{gas})} \quad (14)$$

We have chosen three different feed mole ratios for both gases, following the approach of Shiflett and Yokozeki [18], whose results will be used for comparison. As a result, the CO_2/SO_2 selectivity is plotted in Fig. 10a as a function of the $[C_4mim][MeSO_4]$ concentration at $T=298.15$ K, $P=0.1$ MPa and three CO_2/SO_2 mole ratios (1/9, 1/1, and 9/1). Although the qualitative behavior is similar to that obtained by Shiflett and Yokozeki [18], higher selectivity values are predicted, especially at low concentrations of IL, by the soft-SAFT model. The ternary mixture with the highest SO_2 concentration ($CO_2/SO_2=1/9$, line with circles) significantly increases the selectivity with the addition of IL, moving from 180 to 375 approximately. The increase in selectivity with the IL concentration is also important, although less pronounced, for an equimolar gas feed ratio (passing from 240 to 390 approximately). Finally, the CO_2 rich feed ratio ($CO_2/SO_2=9/1$, line with squares) experiments only a slight to moderate increase with the addition of more IL (from 340 to 390). In this latter case, however, we have not found the maximum in the selectivity value shown in the work of Shiflett and Yokozeki for the rich CO_2 feed ratio. While the selectivity remains quite independent of the feed ratio at high IL concentrations, the differences at low IL concentrations are notorious. It is important to remark that, in this latter case ($CO_2/SO_2=9/1$), the selectivity is very high even with very small amounts of IL (less than 1%). The difference with respect to the selectivity without IL (estimated by Shiflett and Yokozeki to be in the order of 4–14 at the current conditions [18]) provides an idea of how much improvement is achieved by the addition of $[C_4mim][MeSO_4]$ as a solvent.

We have also checked the influence of the temperature by calculating the selectivity at 333.15 K, as shown in Fig. 10b. The same three feed ratios have been studied. As happened before, the comparison with the results of Shiflett and Yokozeki [18] reveals qualitative agreement, although we obtain again higher selectivity values with the soft-SAFT predictions. In this case, the differences between the selectivity as a function of the initial feed ratio are less pronounced than those exhibited at 298.15 K. In comparison to Fig. 10a, the selectivity decreases with the temperature and also becomes less dependent on the IL concentration. Still with that, there are some interesting remarks. As before, the selectivity of the SO_2 rich feed ratio ($CO_2/SO_2=1/9$, line with circles) increases with the addition of ionic liquid, moving from 112 till 150, approximately. The selectivity of the equimolar gas feed ratio

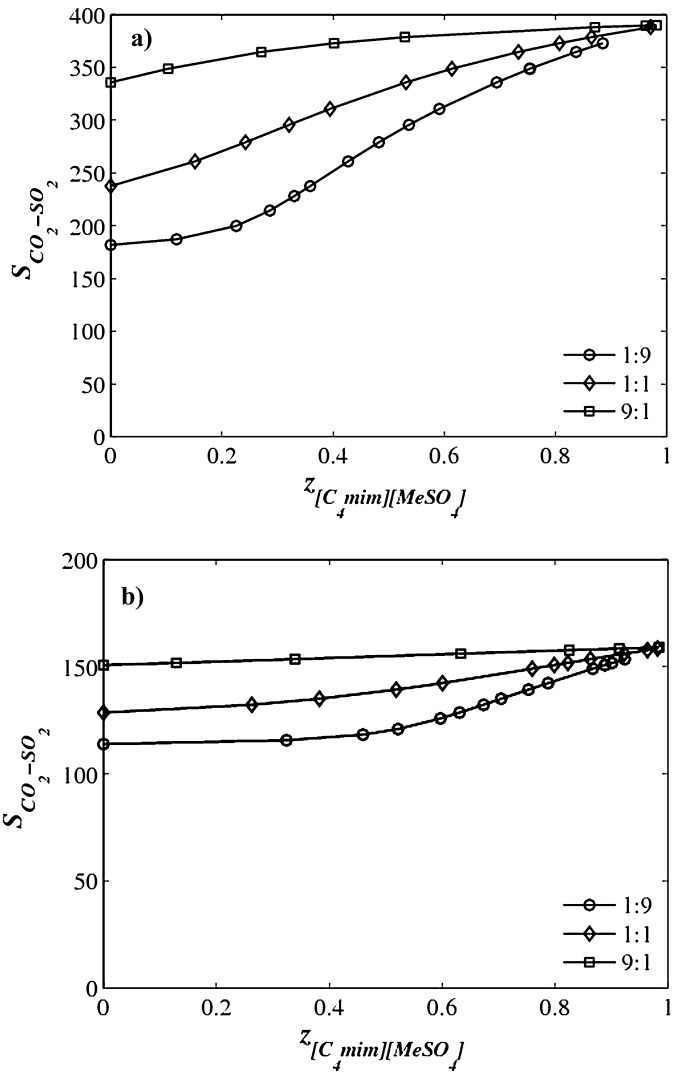

Fig. 10. Selectivity of the CO_2/SO_2 separation as a function of the feed $[C_4mim][MeSO_4]$ mole percent at three different CO_2/SO_2 feed ratios of 1:9 (circles), 1:1 (diamonds) and 9:1 (squares) at (a) $T=298.15$ K and $P=0.1$ MPa, and (b) $T=333.15$ K and $P=0.1$ MPa.

($CO_2/SO_2=1/1$, line with diamonds) increases slightly from 125 till 155, while the selectivity of the CO_2 rich feed ratio ($CO_2/SO_2=9/1$, line with squares) remains practically constant around 150, independent of the IL concentration. The prediction of the CO_2 rich feed ratio deviates from the predictions of Shiflett and Yokozeki, as those authors found that the selectivity was slightly decreasing with the IL concentration. Checking Fig. 10b, it is interesting to note that for small amounts of IL, the selectivity is strongly dependent on the amount of CO_2 and SO_2 present in the flue gas, while at high concentrations, all the mixtures behave very similarly.

As done previously for the CO_2/SO_2 separation, the selectivity of the CO_2/H_2S separation as a function of the addition of IL in the feed flow can be calculated from the ternary diagram using Eq. (14). Once again, three different feed mole ratios for both gases are chosen and compared with the results obtained by Shiflett et al. with the SRK type EoS [19] at 298.15 K and $P=0.1$ MPa. The results are shown in Fig. 11. As it can be observed, lower values than those found for the SO_2 separation are achieved, ranging between 11.1 and 11.3. Moreover, they remain practically constant and independent of the concentration of the IL. The differences among the different feed ratios is very minor, although the higher selectivity is achieved for the H_2S rich feed ratio (CO_2/H_2S 1:9), in contrast with the results

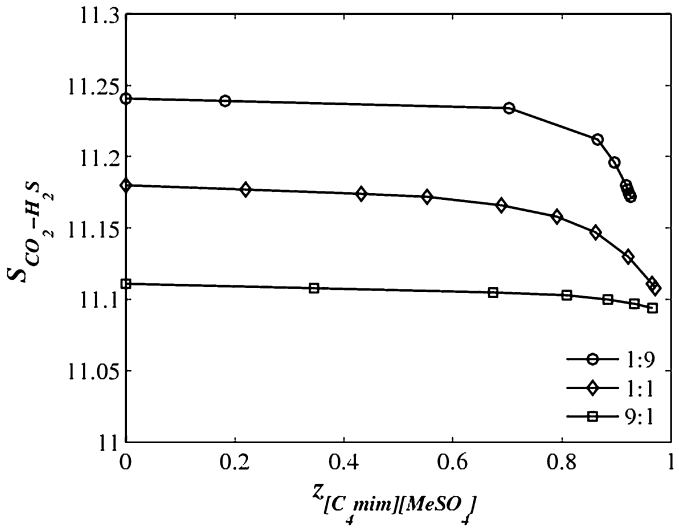

Fig. 11. Selectivity of the CO_2/H_2S separation as a function of the feed $[C_4mim][MeSO_4]$ mole percent at three different CO_2/H_2S feed ratios of 1:9 (circles), 1:1 (diamonds) and 9:1 (squares) at $T = 298.15$ K and $P = 0.1$ MPa.

of Shiflett and co-workers [19], who found that the CO_2 rich feed ratio (CO_2/H_2S 9:1) was providing the highest selectivity (around 13.5). However, it is important to insist on the fact the selectivity values are practically equal in all cases. Compared to the original CO_2/H_2S selectivity without IL (estimated by Shiflett et al. [19] in values between 2 and 4), the improvement is moderate. We have also checked the selectivity of this mixture at a higher temperature (313.15 K), finding very similar results to those shown in Fig. 11. The effect of the temperature is minor. These results have not been included here to avoid repetitiveness.

5. Conclusions

The use of a robust molecular-based equation of state to describe the ability of the $[MeSO_4]$ butyl-imidazolium-based IL for the separation of gases and contaminants has been addressed here. Based on information from previous works, a relatively simple molecular model, where the cation and the anion are considered as a chain, has been proposed for the IL. The model has been used to calculate the solubility of CO_2, CO, H_2, CH_4, SO_2 and H_2S on $[C_4mim][[MeSO_4]$ and has been compared versus available experimental data. Good agreement has been found in a wide range of temperatures and pressures, using only one binary parameter for each gas. A VLLE region has been predicted for the mixtures with CO_2 and H_2S, although the immiscibility area is reduced to a very narrow composition range for the second case. From the binary mixtures, the Henry's constant for each case and the selectivity by respect of CO_2 have been predicted, finding a favorable separation in all cases. For CO, H_2 and CH_4, the separation is given by the absorption of CO_2 in the IL stream, while SO_2 and H_2S are preferentially absorbed and CO_2 remains in the gas phase.

Due to the industrial interest in finding a better solvent for the gas separation of CO_2 from acid gases for the conversion of CO_2, the study has been extended in detail to evaluate the ternary diagrams of the mixtures of CO_2 with SO_2 and H_2S in the IL. For this purpose, the ternary diagrams of the mixtures $SO_2 + CO_2 + [C_4mim][MeSO_4]$ and $H_2S + CO_2 + [C_4mim][MeSO_4]$ have been calculated in a predictive manner in order to obtain additional insight about the best conditions for the separation of these acid gases from carbon dioxide, and to better determine the effect of the immiscibility found in the CO_2 binary mixture. Large areas of immiscibility have been found in both cases, preventing the separation using elevated concentrations of the IL at moderate to high pressures. The selectivity at 298.15 K and atmospheric pressure has been calculated as a function of three different feed ratios and compared to previous studies done by other authors. The results have shown that the conditions studied are suitable for a very favorable separation of CO_2 and SO_2 using $[C_4mim][MeSO_4]$, even at very low concentrations of the IL, as very high selectivity values are achieved. For the H_2S case, only moderate improvements are obtained, giving the idea that there is still some room for improvement by the search of a more suitable solvent.

This work highlights how the molecular modeling methodology can assess the choice of the right solvent in a specific application, a very useful tool when dealing with the design of ILs. Further research is expected to include catalytic processes where the addition of a co-solvent can increase the yield of the product. In particular, high expectations are put in a new class of salts that can overcome the high price of ILs (one of its disadvantages): the study of Deep Eutectic Solvents (DESs), obtained by mixing two safe and cheap compounds that form an eutectic mixture, as potential solvents [46].

Acknowledgements

F. Llovell acknowledges a TALENT fellowship from the Catalan Government. M.B. Oliveira acknowledges for her Post-Doctoral grant (SFRH/BPD/71200/2010). This work has been partially financed by the Catalan government (project 2014-SGR1582), and from Carburos Metálicos (Air Products Group). CICECO is being funded by FCT through project Pest-C/CTM/LA0011/2011.

References

[1] S. Aparicio, M. Atilhan, F. Karadas, Ind. Eng. Chem. Res. 49 (2010) 9580–9595.
[2] Z.-Z. Yang, Y.-N. Zhao, L.-N. He, RSC Adv. 1 (2011) 545–567.
[3] X. Zhang, X. Zhang, H. Dong, Z. Zhao, S. Zhang, Y. Huang, Energy Environ. Sci. 5 (2012) 6668–6681.
[4] A. Olajire, Energy 45 (2010) 2610–2628.
[5] S. Zhang, Y. Chen, F. Li, X. Lu, W. Dai, R. Mori, Catal. Today 115 (2006) 61–69.
[6] P. Lozano, T. de Diego, D. Carrié, M. Vaultier, J.L. Iborra, Chem. Commun. (2002) 692–693.
[7] M. Roth, J. Chromatogr. A 1216 (2009) 1861–1880.
[8] L.F. Vega, O. Vilaseca, F. Llovell, J.S. Andreu, Fluid Phase Equilib. 294 (2010) 15–30.
[9] F.J. Blas, L.F. Vega, Mol. Phys. 92 (1997) 135–150.
[10] J.S. Andreu, L.F. Vega, J. Phys. Chem. C 111 (2007) 16028–16034.
[11] J.S. Andreu, L.F. Vega, J. Phys. Chem. B 112 (2008) 15398–15406.
[12] F. Llovell, E. Valente, O. Vilaseca, L.F. Vega, J. Phys. Chem. B 115 (2011) 4387–4398.
[13] J.D. Holbrey, W.M. Reichert, R.P. Swatloski, G.A. Broker, W.R. Pitner, K.R. Seddon, D.R. Rogers, Green Chem. 4 (2002) 407–413.
[14] S.R. Roy, P.S. Jadhavar, K. Seth, K.K. Sharma, A.K. Chakrabortii, Synthesis 14 (2011) 2261–2267.
[15] J. Kumełan, A. Pérez-Salado Kamps, D. Tuma, G. Maurer, J. Chem. Eng. Data 51 (2006) 1802–1807.
[16] J. Kumełan, A. Pérez-Salado Kamps, D. Tuma, G. Maurer, J. Chem. Eng. Data 52 (2007) 2319–2324.
[17] J. Kumełan, A. Pérez-Salado Kamps, D. Tuma, G. Maurer, Fluid Phase Equilib. 260 (2007) 3–8.
[18] M.B. Shiflett, A. Yokozeki, Energy Fuels 24 (2010) 1001–1008.
[19] M.B. Shiflett, A.M.S. Niehaus, A. Yokozeki, J. Chem. Eng. Data 55 (2010) 4785–4793.
[20] M.B. Shiflett, A. Yokozeki, Ind. Eng. Chem. Res. 49 (2010) 1370–1377.
[21] W.G. Chapman, K.E. Gubbins, G. Jackson, M. Radosz, Ind. Eng. Chem. Res. 29 (1990) 1709–1721.
[22] M.S. Wertheim, J. Stat. Phys. 35 (1984) 35–47.
[23] M.S. Wertheim, J. Stat. Phys. 42 (1986) 459–477.
[24] M.S. Wertheim, J. Stat. Phys. 42 (1986) 477–492.
[25] J.K. Johnson, J.A. Zollweg, K.E. Gubbins, Mol. Phys. 78 (1993) 591–618.
[26] J.K. Johnson, E.A. Müller, K.E. Gubbins, J. Phys. Chem. 98 (1994) 6413–6419.
[27] K.E. Gubbins, C.H. Twu, Chem. Eng. Sci. 33 (1978) 863–878.
[28] P.K. Jog, S.G. Sauer, J. Blaesing, W.G. Chapman, Ind. Eng. Chem. Res. 40 (2001) 4641–4648.
[29] G. Stell, J. Rasaiah, H. Narang, Mol. Phys. 27 (1974) 1393–1414.
[30] F. Llovell, O. Vilaseca, L.F. Vega, Sep. Sci. Technol. 47 (2011) 399–410.
[31] L.J. Florusse, J.C. Pàmies, L.F. Vega, C.J. Peters, H. Meijer, AIChE J. 49 (2003) 3260–3269.

[32] J.C. Pàmies, L.F. Vega, Ind. Eng. Chem. Res. 40 (2001) 2532–2543.
[33] A.M.A. Dias, H. Carrier, J.L. Daridon, J.C. Pàmies, L.F. Vega, J.A.P. Coutinho, I.M. Marrucho, Ind. Eng. Chem. Res. 45 (2006) 2341–2350.
[34] F. Llovell, R.M. Marcos, N. MacDowell, L.F. Vega, J. Phys. Chem. B 116 (2012) 7709–7718.
[35] V.C. Weiss, B. Heggen, F. Müller-Plathe, J. Phys. Chem. C 114 (2010) 3599–3608.
[36] N. Mac Dowell, F. Llovell, N. Sun, J.P. Hallett, A. George, P.A. Hunt, T. Welton, B.A. Simmons, L.F. Vega, J. Phys. Chem. B 118 (2014) 6206–6221.
[37] M.B. Oliveira, F. Llovell, J.A.P. Coutinho, L.F. Vega, J. Phys. Chem. B 116 (2012) 9089–9100.
[38] L.M.C. Pereira, M.B. Oliveira, A.M.A. Dias, F. Llovell, L.F. Vega, P.J. Carvalho, J.A.P. Coutinho, Int. J. Greenh. Gas Control 19 (2013) 299–309.
[39] L.M.C. Pereira, M.B. Oliveira, F. Llovell, L.F. Vega, J.A.P. Coutinho, J. Supercrit. Fluids 92 (2014) 231–241.
[40] F. Llovell, O. Vilaseca, L.F. Vega, Sep. Sci. Technol. 47 (2012) 399–410.
[41] P. Gu, R. Lü, S. Wang, Y. Lu, D. Liu, Comp. Theor. Chem. 1020 (2013) 22–31.
[42] Z. Lei, C. Dai, B. Chen, Chem. Rev. 114 (2014) 1289–1326.
[43] V. Lachet, T. de Bruin, P. Ungerer, C. Coquelet, A. Valtz, V. Hasanov, F. Lockwood, D. Richon, Energy Procedia 1 (2009) 1641–1647.
[44] A. Yokozeki, M.B. Shiflett, Energy Fuels 23 (2009) 4701–4708.
[45] J.A. Bierlein, W.B. Kay, Ind. Eng. Chem. 45 (1953) 618–624.
[46] Q. Zhang, K.D.O. Vigier, S. Royer, F. Jerome, Chem. Soc. Rev. 41 (2012) 7108–7146.